1

The stellar-dynamical search for supermassive black holes in galactic nuclei

JOHN KORMENDY
Department of Astronomy, University of Texas at Austin

Abstract

The robustness of stellar-dynamical black hole (BH) mass measurements is illustrated using six galaxies that have results from independent research groups. Derived BH masses have remained constant to a factor of ~ 2 as spatial resolution has improved by a factor of 2 – 330, as velocity distributions have been measured in increasing detail, and as the analysis has improved from spherical, isotropic models to axisymmetric, three-integral models. This gives us confidence that the masses are reliable and that the galaxies do not indulge in a wide variety of perverse orbital structures. Another successful test is the agreement between a preliminary stellar-dynamical BH mass for NGC 4258 and the accurate mass provided by the maser disk. Constraints on BH alternatives are also improving. In M 31, *Hubble Space Telescope* (*HST*) spectroscopy shows that the central massive dark object (MDO) is in a tiny cluster of blue stars embedded in the P2 nucleus of the galaxy. The MDO must have a radius $r \lesssim 0.''06$. M 31 becomes the third galaxy in which dark clusters of brown dwarf stars or stellar remnants can be excluded. In our Galaxy, spectacular proper motion observations of almost-complete stellar orbits show that the central dark object has radius $r \lesssim 0.0006$ pc. Among BH alternatives, this excludes even neutrino balls. Therefore, measurements of central dark masses and the conclusion that these are BHs have both stood the test of time. Confidence in the BH paradigm for active galactic nuclei (AGNs) is correspondingly high.

Compared to the radius of the BH sphere of influence, BHs are being discovered at similar spatial resolution with *HST* as in ground-based work. The reason is that *HST* is used to observe more distant galaxies. Typical BHs are detectable in the Virgo cluster, and the most massive ones are detectable 3 – 6 times farther away. Large, unbiased samples are accessible. As a result, *HST* has revolutionized the study of BH demographics.

1.1 Introduction

The supermassive black hole paradigm for AGNs was launched by Zel'dovich (1964), Salpeter (1964), and Lynden-Bell (1969, 1978), who argued that the high energy production efficiencies required to make quasars are provided by gravity power. Eddington-limited accretion suggested that BH engines have masses of 10^6 to 10^9 $M_\odot$. Confidence grew rapidly with the amazing progress in AGN observations and with the paradigm's success in weaving these results into a coherent theoretical picture. Unlike the normal course of scientific research, acceptance of the AGN paradigm came long before there was any dynamical evidence that BHs exist.

Table 1.1 *Black Hole Mass Measurements*

Galaxy	D (Mpc)	σ_e (km/s)	$M_\bullet$ ($M_{\rm low}, M_{\rm high}$) ($M_\odot$)	$r_{\rm cusp}$ (arcsec)	σ_* (arcsec)	$r_{\rm cusp}/\sigma_*$	Reference
Galaxy	0.008	103	3.7 (3.3–4.1) e6	38.8	0.0159	2438.	Ghez 2004
Galaxy			3.7 (2.2–5.2) e6		0.0159	2438.	Schödel + 2002
Galaxy			2.0 (1.3–2.7) e6		0.113	343.	Chakrabarty + 2001
Galaxy			3.0 (2.6–3.3) e6		0.26	150.	Genzel + 2000
Galaxy			2.6 (2.4–2.8) e6		0.39	100.	Ghez + 1998
Galaxy			2.6 (2.3–3.0) e6		0.39	100.	Genzel + 1997
Galaxy			2.5 (2.1–2.9) e6		0.39	100.	Eckart + 1997
Galaxy			2.7 (2.4–3.0) e6		2.60	14.9	Genzel + 1996
Galaxy			1.8 (1.3–2.3) e6		3.6	10.8	Haller + 1996
Galaxy			2.8 (1.9–3.8) e6		3.4	11.4	Krabbe + 1995
Galaxy			2. e6		5.2	7.5	Evans + 1994
Galaxy			3. e6		5.2	7.5	Kent 1992
Galaxy			5.2 (3.8–6.6) e6		5.2	7.5	Sellgren + 1990
M 31			1.0 e8		0.297	10.8	Peiris + 2004
M 31	0.76	160	7.0 (3.0–20.0) e7	3.20	0.039	81.	Bender + 2004
M 31			7.0 (3.5–8.5) e7		0.052	61.	Bacon + 2001
M 31			3.3 (1.5–4.5) e7		0.297	10.8	Kormendy + 1999
M 31			5.9 (5.7–6.1) e7		0.297	10.8	Magorrian + 1998
M 31			7.4 e7		≈ 0.57	≈ 5.6	Tremaine 1995
M 31			7.8 e7		0.39	8.2	Bacon + 1994
M 31			5.0 (4.4–5.5) e7		0.60	5.3	Richstone + 1990
M 31			3.6 (1.1–10.9) e7		0.57	5.6	Kormendy 1988a
M 31			7.7 (3.3–7.7) e7		0.60	5.3	Dressler + 1988
M 32	0.81	75	2.9 (2.3–3.5) e6	0.56	0.052	10.83	Verolme + 2002
M 32			3.7 (2.6–5.0) e6		0.052	10.83	Joseph + 2001
M 32			2.4 (2.2–2.6) e6		0.23	2.41	Magorrian + 1998
M 32			4.0 (3.1–4.8) e6		0.050	11.39	van der Marel + 1998b
M 32			4.0 (2.1–5.8) e6		0.050	11.39	van der Marel + 1997ab
M 32			3.2 (2.6–3.7) e6		0.23	2.41	Bender + 1996
M 32			2.1 (1.9–2.3) e6		0.34	1.66	Dehnen 1995
M 32			2.1 e6		0.34	1.66	Qian + 1995
M 32			2.1 (1.7–2.4) e6		0.34	1.66	van der Marel + 1994b
M 32			2.2 (0.8–3.5) e6		0.59	0.95	Richstone + 1990
M 32			9.4 (4.7–18.9) e6		0.59	0.95	Dressler + 1988
M 32			7.6 (3.5–11.6) e6		0.76	0.75	Tonry 1987
M 32			5.9 e6		1.49	0.38	Tonry 1984
M 81	3.9	143	6.8 (5.5–7.5) e7	0.76	0.068	11.08	Bower + 2000
NGC 821	24.1	209	3.7 (2.9–6.1) e7	0.031	0.052	0.60	Gebhardt + 2003
NGC 1023	11.4	205	4.4 (3.9–4.8) e7	0.081	0.068	1.18	Bower + 2001
NGC 2778	22.9	175	1.4 (0.5–2.2) e7	0.018	0.052	0.34	Gebhardt + 2003
NGC 3115	9.7	182	1.0 (0.4–2.0) e9	2.77	0.047	59.	Tremaine + 2002
NGC 3115			6.3 (2.9–9.7) e8		0.111	24.9	Emsellem + 1999
NGC 3115			4.7 (4.4–4.9) e8		0.26	10.6	Magorrian + 1998
NGC 3115			1.5 e9		0.047	59.	Kormendy + 1996a
NGC 3115			1.6 (1.1–2.1) e9		0.50	5.5	Kormendy + 1992
NGC 3377			5.7 (3.4–11.) e7		0.29	1.3	Cretton + 2004
NGC 3377	11.2	145	1.0 (0.9–1.9) e8	0.38	0.111	3.4	Gebhardt + 2003
NGC 3377			6.9 (6.3–7.7) e7		0.24	1.57	Magorrian + 1998
NGC 3377			2.0 (1.1–2.9) e8		0.24	1.57	Kormendy + 1998
NGC 3379	10.6	206	1.0 (0.6–2.0) e8	0.201	0.111	1.81	Gebhardt + 2000a
NGC 3384	11.6	143	1.6 (1.4–1.7) e7	0.060	0.052	1.15	Gebhardt + 2003
NGC 3608	22.9	182	1.9 (1.3–2.9) e8	0.223	0.052	4.3	Gebhardt + 2003
NGC 4258	7.2	105	2.0 (1.0–3.0) e7	0.44	0.052	8.4	Siopis + 2004

Table 1.1 *Black Hole Mass Measurements*

Galaxy	D (Mpc)	σ_e (km/s)	$M_\bullet$ ($M_{\rm low}, M_{\rm high}$) ($M_\odot$)	$r_{\rm cusp}$ (arcsec)	σ_* (arcsec)	$r_{\rm cusp}/\sigma_*$	Reference
NGC 4291	26.2	242	3.1 (0.8–3.9) e8	0.180	0.052	3.45	Gebhardt + 2003
NGC 4342	15.3	225	3.1 (2.0–4.8) e8	0.351	0.135	2.60	Cretton + 1999a
NGC 4473	15.7	190	1.1 (0.3–1.5) e8	0.173	0.052	3.31	Gebhardt + 2003
NGC 4486B	16.1	185	6.0 (4.0–9.0) e8	0.97	0.258	3.75	Kormendy + 1997
NGC 4564	15.0	162	5.6 (4.8–5.9) e7	0.127	0.052	2.43	Gebhardt + 2003
NGC 4594			6.9 (6.7–7.0) e8		0.46	3.78	Magorrian + 1998
NGC 4594	9.8	240	1.1 (0.3–3.4) e9	1.73	0.111	15.61	Kormendy + 1996b
NGC 4594			5.4 (4.9–6.0) e8		0.46	3.78	Emsellem + 1994
NGC 4594			5.4 (1.7–17.2) e8		0.46	3.78	Kormendy 1988b
NGC 4649	16.8	385	2.0 (1.4–2.4) e9	0.71	0.052	13.71	Gebhardt + 2003
NGC 4697	11.7	177	1.7 (1.6–1.9) e8	0.41	0.052	7.9	Gebhardt + 2003
NGC 4742	15.5	90	1.4 (0.9–1.8) e7	0.099	0.068	1.45	Kaiser + 2004
NGC 5845	25.9	234	2.4 (1.0–2.8) e8	0.150	0.111	1.36	Gebhardt + 2003
NGC 7457	13.2	67	3.5 (2.1–4.6) e6	0.053	0.052	1.01	Gebhardt + 2003
IC 1459	29.2	340	2.5 (2.1–3.0) e9	0.661	0.052	12.69	Cappellari + 2002
NGC 2787	7.5	140	4.1 (3.6–4.5) e7	0.248	0.068	3.63	Sarzi + 2001
M 81	3.9	143	7.5 (6.4–9.7) e7	0.76	0.052	14.6	Devereux + 2003
NGC 3245	20.9	205	2.1 (1.6–2.6) e8	0.213	0.068	3.11	Barth + 2001
NGC 4261	31.6	315	5.2 (4.1–6.2) e8	0.146	0.058	2.54	Ferrarese + 1996
NGC 4374	18.4	296	1.6 (0.4–2.8) e9	0.89	0.068	13.1	Bower + 1998
NGC 4459	16.1	186	7.0 (5.7–8.3) e7	0.112	0.068	1.63	Sarzi + 2001
M 87	16.1	375	3.4 (2.5–4.4) e9	1.35	0.043	31.3	Macchetto + 1997
M 87			2.6 (1.8–3.3) e9		0.135	9.98	Harms + 1994
NGC 4596	16.8	152	7.8 (4.5–11.6) e7	0.179	0.068	2.61	Sarzi + 2001
NGC 5128	4.2	150	2.4 (0.7–6.0) e8	2.26	0.205	11.03	Marconi + 2001
NGC 6251	93	290	5.3 (3.7–6.8) e8	0.060	0.050	1.21	Ferrarese + 1999
NGC 7052	58.7	266	3.3 (2.0–5.6) e8	0.071	0.135	0.52	van der Marel + 1998a
NGC 1068	15	151	1.5 e7	0.039	0.008	4.8	Greenhill + 1997a
NGC 4258	7.2	105	3.9 (3.8–4.0) e7	0.44	0.0047	93.	Herrnstein + 1999
NGC 4945	3.7		1.4 e6				Greenhill + 1997b

Parameters – Column 2 is the distance (Tonry et al. 2001). Column 3 is the galaxy's velocity dispersion outside the sphere of influence of the BH. Column 4 is the BH mass $M_\bullet$ with error bars ($M_{\rm low}, M_{\rm high}$) from the sources in Column 8 corrected to the adopted distance. The line with all columns filled in contains the adopted BH mass. Column 5 is the radius of the sphere of influence of the BH, $r_{\rm cusp} = G\,M_\bullet/\sigma_e^2$. Column 6 is the effective spatial resolution of the spectroscopy (see §1.3.1). Column 7 is the measure of spatial resolution that shows how much leverage the observations have on the BH detection and mass measurement. Parameters not credited are from Tremaine et al. (2002) or from Kormendy & Gebhardt (2001). Notes on individual objects:

Galaxy: For Ghez (2004) and Schödel et al. (2002), σ_* is the pericenter orbital radius of star S2. Otherwise, it is the radius for the centermost radial bin of stars used in the mass analysis.

M 81 and NGC 4258: $M_\bullet$ is adopted from Bower et al. (2000) and Herrnstein et al. (1999).

NGC 3115: Kormendy & Richstone (1992) provide σ_e. The resolution σ_* for Kormendy et al. (1996a) is based on the size of the nuclear star cluster, not on the *HST* spectroscopy. The corresponding BH mass is given by the virial theorem applied to this nucleus (see their §6). Anders et al. (2001) modeled published data and their ground-based, integral field spectroscopy. Isotropic models implied $M_\bullet \simeq 10^9\ M_\odot$, consistent with previous results. However, they find that "anisotropic models reduce this to ca. $2 \times 10^7\ M_\odot$." This is inconsistent with our conclusion from the escape velocity argument that $M_\bullet \approx 10^9\ M_\odot$, independent of anisotropy. Therefore, pending publication of the details of the the Anders et al. (2001) preliminary work, I omit this result.

NGC 4374: I adopted $M_\bullet$ from Bower et al. (1998), but the low-$M_\bullet$ error bar includes the value suggested by Maciejewski & Binney (2001).

For the maser galaxies, σ_* is the radius of the innermost maser source used in the analysis.

The stellar-dynamical BH search began with two papers on M 87 by Young et al. (1978) and by Sargent et al. (1978). Based on the non-isothermal (cuspy) surface brightness profile of its core and an observed rise in velocity dispersion toward the center, they showed that M 87 contains an $M_\bullet \simeq 4 \times 10^9\ M_\odot$ MDO if the stellar velocity distribution is isotropic. At about the same time, it became clear that almost no giant ellipticals like M 87 are isotropic (e.g., Illingworth 1977; Binney 1978) and that anisotropic models can explain the cuspy core and the dispersion gradient without a BH (Duncan & Wheeler 1980; Binney & Mamon 1982; Richstone & Tremaine 1985; Dressler & Richstone 1990). Nevertheless, the Young and Sargent papers were seminal. They set the field in motion.

The dynamical detection of dark objects in galaxy centers began with the discovery of an $M_\bullet \approx 10^{6.5}\ M_\odot$ mass in M 32 (Tonry 1984, 1987; Dressler & Richstone 1988), a $10^{7.5}\ M_\odot$ object in M 31 (Dressler & Richstone 1988; Kormendy 1988a), and $10^9\ M_\odot$ objects in NGC 4594 (Kormendy 1988b) and NGC 3115 (Kormendy & Richstone 1992). The observations were ground-based with resolution FWHM $\approx 1''$. The BH case in our Galaxy developed slowly (see Genzel, Hollenbach, & Townes 1994; Kormendy & Richstone 1995 for reviews), for two reasons. Dust extinction made it necessary to use infrared techniques that were just being developed in the early 1990s. And the $M_\bullet$ measurement in our Galaxy requires the study of a relatively small number of stars that are bright enough to be observed individually. As a result, graininess in the light and velocity distributions becomes a problem. On the other hand, the Galactic Center is very close, so progress in the past decade has been spectacular. Now the Galaxy is by far the best supermassive BH case (§ 1.3.2).

The BH search speeded up dramatically once *HST* provided spatial resolution a factor of 3 to 10 better than ground-based telescopes (see Kormendy & Gebhardt 2001 for a review). By now, almost all galaxies in which BHs were discovered from the ground have undergone several iterations of improved spatial resolution. Analysis machinery has improved just as dramatically. This is an opportune time to take stock of the past 15 years of progress. Are the detections of central dark objects reliable? Are the derived masses robust? And are the dark objects really BHs? The BH search is starting to look like a solved problem; assuming this, emphasis has shifted to demographic studies of BHs and their relation to galaxy evolution (see Richstone et al. 1998; Ho 1999; Kormendy & Gebhardt 2001; Richstone 2004 for reviews). Is this a reasonable attitude? Sanity checks are the purpose of this paper.

1.2 The History of BH Mass Measurements

The history of supermassive BH mass measurements is summarized in Table 1.1. In focusing on this history, I will be concerned with whether we achieve approximately the accuracies that we believe. That is, I concentrate on errors of $\gtrsim 0.2$ dex. To what extent hard work can further squeeze the measurement errors is discussed by Gebhardt (2004).

In Table 1.1, horizontal lines separate BH detections based on stellar dynamics (first group), ionized gas dynamics (middle), and maser dynamics (last group). All multiple stellar-dynamical $M_\bullet$ estimates for the same galaxy are listed. Our Galaxy, M 31, M 32, NGC 3115, NGC 3377, and NGC 4594 have all been measured by at least two competing groups. M 81 has been observed independently in stars and ionized gas; both measurements are listed and they agree. However, consistency checks of $M_\bullet$ values based on ionized gas dynamics have revealed some problems in other galaxies; these are discussed by Maciejewski & Binney (2001), Barth et al. (2001), Verdoes Kleijn et al. (2002), Barth (2004), and Sarzi (2004). I have not included all multiple measurements based on ionized gas dynamics.

1.3 How Robust Are Stellar-Dynamical BH Mass Estimates?

1.3.1 The History of the BH Search As Seen Through Work on M 32

M 32 was the first application of many improvements in spatial resolution, in kinematic analysis techniques, and in dynamical modeling machinery. It provides an excellent case study for a review of these developments. Figure 1.1 illustrates the remarkable result that BH mass estimates for M 32 have remained stable for more than 15 years while a variety of competing groups have improved the observations and analysis*.

The BH in M 32 was discovered as early as possible, when the spatial resolution was so poor that $r_{\rm cusp}/\sigma_* < 1$. This is not surprising, given the importance of the problem. In astronomy as in other sciences, if you wait for a 5 σ result, someone else is likely to make the discovery when it is still a 2 σ result. The trick is to be careful enough to get the right answer even when the result is uncertain. Tonry (1984, 1987) got within a factor of 2.5 of the current best BH mass even though he made serious simplifying assumptions. His spectra did not resolve the intrinsic velocity dispersion gradient near the center; rotational line broadening accounted for the apparent dispersion gradient. Without an intrinsic dispersion gradient, his models were guaranteed not to be self-consistent, because there was no dynamical support in the axial direction. Despite this approximation, Tonry derived $M_\bullet \simeq (6 \text{ to } 8) \times 10^6\ M_\odot$, close to the modern value. Poor spatial resolution allowed considerable freedom to interpret dispersion gradients as unresolved rotation; since V and σ contribute comparably to the dynamical support, trading one for the other results in no large change in $M_\bullet$.

The spatial resolution of the spectroscopy improved by a factor of 30 from the discovery observations (Tonry 1984) to the Space Telescope Imaging Spectrograph (STIS) data from *HST*. In Column 6 of Table 1.1, the Gaussian dispersion radius of the PSF is estimated as follows. First, I estimate the resolution in the directions parallel and perpendicular to the slit as $\sigma_{*\|}$, the sum in quadrature of the radius $\sigma_{*\rm tel}$ of the telescope PSF and of 1/2 pixel, and $\sigma_{*\perp}$, the sum in quadrature of the radius of the telescope PSF and half of the slit width. The *HST* PSF was modeled in van der Marel, de Zeeuw, & Rix (1997b) as the sum of three Gaussians; for all *HST* observations, I use $\sigma_{*\rm tel} \simeq 0\farcs036$, the best single Gaussian dispersion radius that fits this sum. Finally, the effective σ_* is the geometric mean of $\sigma_{*\|}$ and $\sigma_{*\perp}$. I do not take into account slit centering errors; for some observations, these are larger than σ_*.

* The referee suggests that this result is caused by two effects that accidentally cancel because spatial resolution and dynamical models have improved in parallel. He suggests (1) that $M_\bullet$ estimates increase with improving spatial resolution because we reach farther into the BH sphere of influence and (2) that $M_\bullet$ estimates decrease as dynamical models get more sophisticated because the models have more freedom to tinker the orbital structure to fit the data without a BH. I disagree. (1) Reaching farther into the BH sphere of influence should not change $M_\bullet$ if we model the stellar dynamics adequately well. Instead, we should get more "leverage" and smaller mass error bars. Of course, if we model the physics incorrectly, then more leverage may result in a systematic change in $M_\bullet$. But the change could go either way, depending on how the models err in approximating the true velocity anisotropy. In fact, Figure 1.4 shows that improving the spatial resolution does not increase the $M_\bullet$ values given by the Gebhardt et al. (2003) three-integral models, although it does, as expected, improve the error bars. For the Magorrian et al. (1998) models, improving the resolution decreases $M_\bullet$, an effect opposite to that predicted by the referee. (2) Improving modeling techniques provides more degrees of freedom on the orbital structure, but modeling programs do not have any built-in desire to decrease the BH mass. Instead, they have instructions to fit the data. Again, if the real orbital structure is sufficiently well approximated by simple models, then making the models more complicated will not change the BH mass. And if the orbital structure is not well approximated by the simple models, then better models could just as easily increase $M_\bullet$ as decrease it. However, the low-mass error bar on $M_\bullet$ will decrease, for the reason the referee suggests. The high-mass error bar will increase. As a result, the error bars become larger and more realistic. This effect is evident in Table 1.1. I conclude that the consistency of $M_\bullet$ estimates in Figures 1.1 and 1.2 tells us something important, namely that we have been modeling the stellar dynamics of power-law galaxies well enough to derive robust BH masses.

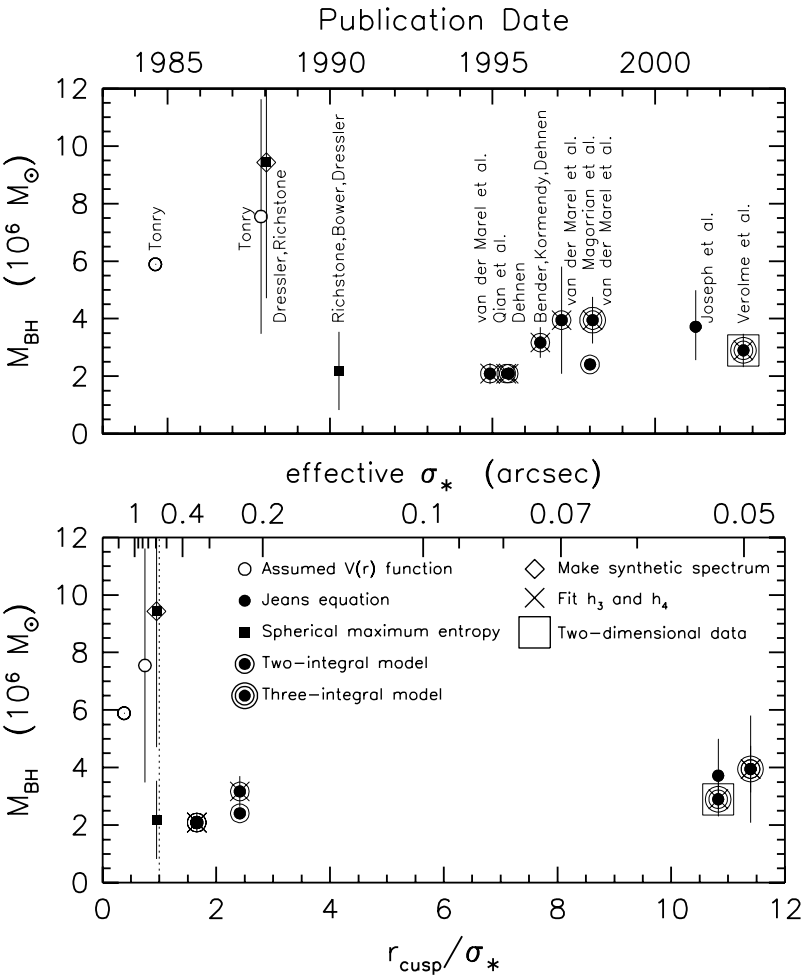

Fig. 1.1. History of the stellar-dynamical BH search as seen through work on M 32: derived BH mass as a function of (top) publication date and (bottom) spatial resolution. Resolution is measured along the top axis by the Gaussian dispersion radius σ_* of the effective PSF (see text). More relevant physically (bottom axis) is the ratio of the radius of the sphere of influence of the BH, $r_{\rm cusp} = GM_\bullet/\sigma^2$, to σ_*. If $r_{\rm cusp}/\sigma_* \lesssim 1$, then the measurements are dominated by the mass distribution of the stars rather than by the BH. If $r_{\rm cusp}/\sigma_* \gg 1$, then we reach well into the part of the galaxy where velocities are dominated by the BH. Symbols shapes encode improvements in observations or kinematic measurements (right key) and in dynamical modeling techniques (left key). The data are listed in Table 1.1.

Dressler & Richstone (1988) and Richstone, Bower, & Dressler (1990) followed with better observations and analysis. They fitted spherical maximum entropy models including velocity anisotropy. By this time, it was well known that unknown velocity dispersion anisotropy was the biggest uncertainty in $M_\bullet$ measurements based on stellar dynamics. They were unable to explain the central kinematic gradients in M 32 without a BH. Rapid confirmation of Tonry's BH detection contributed to the early acceptance of this subject.

Since then, dynamical modeling machinery has improved remarkably. The next major

step defined the state of the art from 1995 through 1997. This was the use of two-integral models that included flattening and velocity dispersion anisotropy. Essentially simultaneous work by van der Marel et al. (1994b), Qian et al. (1995), and Dehnen (1995) all derived $M_\bullet = 2.1 \times 10^6\ M_\odot$ from van der Marel's data. Soon thereafter, Bender, Kormendy, & Dehnen (1996) got $3.2 \times 10^6\ M_\odot$ using the same machinery on CFHT data of slightly higher resolution. The limitation of these models, as the authors realized, was the fact that two-integral models are approximations. They work best for cuspy and relatively rapidly rotating galaxies like M 32, but they are not fully general. Still, by this time, it was routine to measure not just the first two moments of the line-of-sight velocity distributions (LOSVDs)—that is, V and σ—but also the next two coefficients h_3 and h_4 in a Gauss-Hermite expansion of the LOSVDs. These measure asymmetric and symmetric departures from Gaussian line profiles. In a transparent galaxy that rotates differentially, projection guarantees that $h_3 \neq 0$. In general, h_3 is antisymmetric with V. A galaxy containing a BH is likely to have $h_4 > 0$; that is, an LOSVD that is more centrally peaked than a Gaussian. The reason is that stars close to the BH move very rapidly and give the LOSVD broader symmetric wings than they would otherwise have (van der Marel 1994). Thus, as emphasized especially by van der Marel et al. (1994a), measuring and fitting h_3 and h_4 adds important new constraints both to the stellar distribution function and to the BH detection and mass determination.

HST Faint Object Spectrograph (FOS) observations of M 32 were obtained by van der Marel et al. (1998b). These authors further "raised the bar" on BH mass measurements by fitting their data with three-integral dynamical models constructed using Schwarzschild's (1979) method. Such models now define the state of the art (see Cretton et al. 1999b; Gebhardt et al. 2000a, 2003; Richstone et al. 2004 for more detail).

Finally, the most thorough data set and modeling analysis for M 32 is provided by Verolme et al. (2002). They use the SAURON two-dimensional spectrograph to measure V, σ, h_3, and h_4 in the central $9'' \times 11''$. Also, *HST* STIS spectroscopy (Joseph et al. 2001) provides improved data near the BH. These observations fitted with three-integral models for the first time break the near-degeneracy between the stellar mass-to-light ratio, M/L, and the unknown inclination of the galaxy. Because the mass in stars is better known, the BH mass is more reliable. Again, the derived BH mass is similar to that given in previous analyses, $M_\bullet = (2.9 \pm 0.6) \times 10^6\ M_\odot$.

So the BH mass derived for M 32 has remained almost unchanged while the observations and analysis have improved dramatically. It was exceedingly important to our confidence in the BH detection to test whether the apparent kinematic gradients near the center could be explained without a BH. Asked to do this, a dynamical modeling code attempts to fine-tune the stellar velocity dispersion anisotropy. In general, it tries to add more radial orbits near the center, because doing so implies less mass for the same σ. Nowadays, its freedom to tinker is severely restricted by the need to match the full LOSVDs. However, even simple approximations to the dynamical structure gave essentially the correct BH mass. *That is, M 32 does not use its freedom to indulge in perverse orbit structure.* The following sections show that this is also true in our Galaxy, M 31, NGC 3117, NGC 3377, and NGC 4594. Dynamical mass modeling is relatively benign in such galaxies that have power-law profiles (for more details, see Kormendy et al. 1994; Lauer et al. 1995; Gebhardt et al. 1996; Faber et al. 1997; Lauer 2004). It would not be safe to assume that this result applies equally well to galaxies with cuspy cores.

1.3.2 The Best Case of a Supermassive Black Hole: Our Galaxy

Figure 1.2 summarizes the history of BH mass measurements in galaxies with observations or stellar-dynamical mass analyses by different research groups. The BH case that has improved the most is the one in our Galaxy. Both the evidence for a central dark object and the arguments that this is a BH and not something less exotic like a cluster of dark stars are better in our Galaxy than anywhere else.

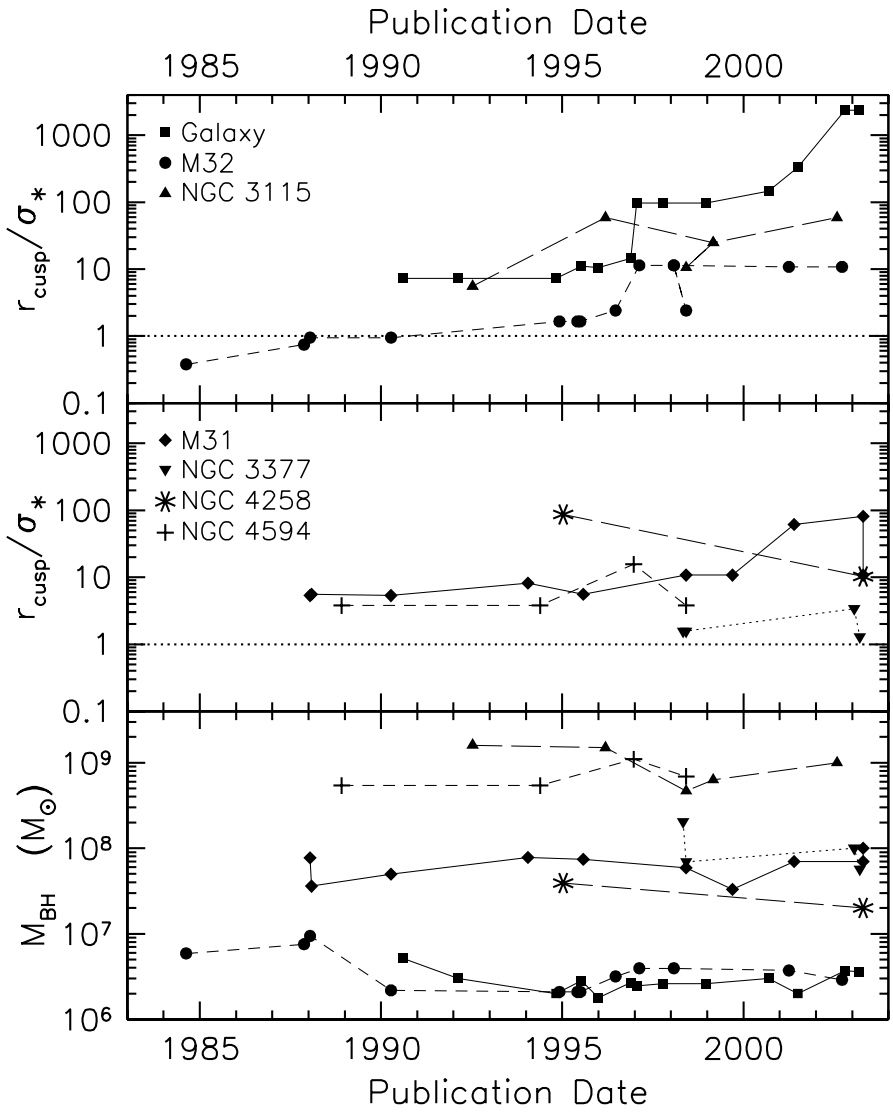

Fig. 1.2. Effective resolution of the best spectroscopy (top two panels) and resulting BH mass estimates (bottom) versus publication date. The data are listed in Table 1.1. For M 31 and M 32, steep rises in r_{cusp}/σ_* occur when *HST* was first used to observe the galaxies. For our Galaxy, two jumps in r_{cusp}/σ_* occur when the kinematic work switched from radial velocities to proper motions in the Sgr A* star cluster and when the first nearly complete stellar orbit in that cluster was observed.

A complete review of the BH search in our Galaxy is beyond the scope of this paper. Early work is discussed in Genzel & Townes (1987); Genzel et al. (1994); Kormendy & Richstone (1995), and in conference proceedings such as Backer (1987), Morris (1989), and Genzel & Harris (1994). Observations of our Galactic Center benefit from the fact that it is 100 times closer than the next nearest good BH cases, M 31 and M 32. For a distance of 8 kpc, the scale is $25\farcs8$ pc^{-1}. Early gas- and stellar-dynamical studies suggested the presence of a several-million-solar-mass dark object. In Table 1.1 and Figure 1.2, I date the convincing case for a BH to Sellgren et al. (1990) and to Kent (1992). Since then, two dramatic improvements in spatial resolution have taken place.

Research groups led by Reinhard Genzel and Andrea Ghez have pioneered the use of speckle interferometry and, more recently, adaptive optics imaging and spectroscopy to achieve spatial resolutions good enough to resolve a tiny cluster of stars (radius $\sim 1''$) that surrounds the compact radio source Sgr A* at the Galactic Center. The Sgr A* cluster is so tiny that stars move fast enough to allow us to observe proper motions. This provides a direct measure of the velocity dispersion anisotropy. It is not large. The derived central mass is about $2.5 \times 10^6\ M_\odot$. And, even though the number density of stars is higher than we observe anywhere else, the volume is so small that the stellar mass is negligible. The advent of proper motion measurements accounts for the jump in $r_{\rm cusp}/\sigma_*$ at the start of 1997.

A second jump in $r_{\rm cusp}/\sigma_*$ has just occurred as a result of an even more remarkable observational coup. As reviewed in this volume by Ghez (2004), Schödel et al. (2002), Ghez et al. (2003), and Ghez (1994) have independently measured several individual stellar orbits through pericenter passage. In the case of star S2, more than half of an orbit has been observed (period = 15.78 $\pm$ 0.82 years). The orbit is closed, so the controlling mass resides inside $r_{\rm peri} \simeq 0\farcs0159 \simeq 0.00062$ pc $\simeq$ 127 AU $\simeq$ 1790 Schwarzschild radii. This accounts for the current jump in spatial resolution. As measurement accuracies improve, the observation of individual closed orbits will rapidly obsolete the complicated analysis of stellar distribution functions that describe ensembles of stars at larger radii. Rather, the analysis will acquire the much greater rigor inherent in the two-body problem. Arguably the orbit of S2 already contributes as much to our confidence in the BH detection as all stars at larger radii combined. The best-fitting BH mass, $M_\bullet = (3.7 \pm 0.4) \times 10^6\ M_\odot$, is in good agreement with, but slightly larger than, the value derived from the stellar-dynamical modeling. This leads to an important point: The above comparison in our Galaxy and a similar one in NGC 4258 (see the next section) are currently the only reliable external checks on our stellar-dynamical modeling machinery. The measurement accuracies are not good enough yet to show whether the models achieve the accuracies that we expect for the best data ($\pm$30%: Gebhardt 2004). But neither test points to modeling errors that range over a factor of ~ 6 as feared by Valluri, Merritt, & Emsellem (2004).

Finally, these new observations have an implication that is actually more fundamental than the mass measurement. They restrict the dark mass to live inside such a small radius that even neutrino balls (Tsiklauri & Viollier 1998, 1999; Munyaneza, Tsiklauri, & Viollier 1998, 1999; Munyaneza & Viollier 2002) with astrophysically allowable neutrino masses are excluded. The exclusion principle forces them to be too fluffy to be consistent with the radius constraints. Dark clusters of brown dwarf stars or stellar remnants were already excluded (Maoz 1995, 1998)—brown dwarfs would collide, merge, and become visible stars, and stellar remnants would evaporate via relaxation processes. The maximum lifetime of dark cluster alternatives to a BH is now a few times 10^5 yr (Schödel et al. 2002).

1.3.3 The Best Test of Stellar-Dynamical $M_\bullet$ Estimates: NGC 4258

The galaxy that stands out as having the most reliable BH mass measurement is NGC 4258. Very Long Baseline Array measurements of its nuclear water maser disk reach to within 0.″0047 = 0.16 pc of the BH (Miyoshi et al. 1995). The rotation curve, $V(r) = 2180\ (r/0.''001)^{-1/2}$ km s^{-1}, is Keplerian to high precision. Proper motion and acceleration observations of the masers in front of the Seyfert nucleus are consistent with the radial velocity measurements along the orbital tangent points (Herrnstein et al. 1999). All indications are that the rotation is circular. Therefore $M_\bullet = (3.9 \pm 0.1) \times 10^7\ M_\odot$ is generally regarded as bomb-proof.

This provides a unique opportunity to test the three-integral dynamical modeling machinery used by the Nuker team (Gebhardt et al. 2000a, b, 2003; Richstone et al. 2004). NGC 4258 contains a normal bulge much like the one in M 31 (Kormendy et al. 2004a). Siopis et al. (2004) have obtained *HST* STIS spectra and WFPC2 images of NGC 4258. The STIS spectroscopy has spatial resolution $r_{\rm cusp}/\sigma_* \simeq 8.4$ well within the range of the BH discoveries in Table 1.1. The kinematic gradients are steep, consistent with the presence of a BH. Three-integral models are being calculated as I write this; the preliminary result is that $M_\bullet = (2 \pm 1) \times 10^7\ M_\odot$. The agreement with the maser $M_\bullet$ is fair. The problem is the brightness profile, which involves more complications than in most BH galaxies. A color gradient near the center may be a sign of dust obscuration, and correction for the bright AGN (Chary et al. 2000) is nontrivial. Both problems get magnified by deprojection.

1.3.4 A Case History of Improving Spatial Resolution: NGC 3115

One sanity check on BH detections is that apparent kinematic gradients should get steeper as the spectroscopic resolution improves. We have seen this test work in M 32 and in our Galaxy. This section is a brief discussion of NGC 3115. At $r_{\rm cusp}/\sigma_* = 59$, NGC 3115 is surpassed in spectroscopic resolution only by our Galaxy, NGC 4258, and M 31.

Exploiting the good seeing on Mauna Kea, Kormendy & Richstone (1992) found a central dark object of $10^9\ M_\odot$ in NGC 3115 using the Canada-France-Hawaii Telescope (CFHT). The resolution was not marginal; $r_{\rm cusp}/\sigma_* \simeq 5.5$. This is higher than the median for *HST* BH discoveries in Figure 1.3 (§ 1.3.7). Since then, there have been two iterations in improved spectroscopic resolution (Kormendy et al. 1996a). The apparent central velocity dispersion increased correspondingly: it was $\sigma = 295 \pm 9$ km s^{-1} at $r_{\rm cusp}/\sigma_* \simeq 5.5$, $\sigma = 343 \pm 19$ km s^{-1} at $r_{\rm cusp}/\sigma_* \simeq 10.6$ (CFHT plus Subarcsecond Imaging Spectrograph), and $\sigma = 443 \pm 18$ km s^{-1} at $r_{\rm cusp}/\sigma_* \simeq 59$ (*HST* FOS). These are projected velocity dispersions: they include the contribution of foreground and background stars that are far from the BH and so have relatively small velocity dispersions. However, NGC 3115 has a tiny nuclear star cluster that is very distinct from the rest of the bulge. It is just the sort of high-density concentration of stars that we always expected to find around a BH. From a practical point of view, it is a great convenience, because it is easy to subtract the foreground and background light as estimated from the spectra immediately adjacent to the nucleus. This procedure is analogous to sky subtraction. It provides the velocity dispersion of the nuclear cluster by itself and is, in effect, another way to increase the spatial resolution. The result is that the nuclear cluster has a velocity dispersion of $\sigma = 600 \pm 37$ km s^{-1}. The effective spatial resolution of this measurement is not determined by the spectrograph but rather by the half-radius $r_h = 0.''052 \pm 0.''010$ of the nuclear cluster. This is smaller than the entrance aperture of the FOS. It implies that $r_{\rm cusp}/\sigma_* \simeq 59$, as quoted in Table 1.1.